Breakup of H_2^+ by photon impact

Daniel J. Haxton

Chemical Sciences, Lawrence Berkeley National Laboratory, Berkeley, California 94720, USA

Total and partial cross sections for breakup of the ground rovibronic state of H_2^+ by photon impact are calculated using the exact nonadiabatic nonrelativistic Hamiltonian without approximation. The converged results span six orders of magnitude. The breakup cross section is divided into dissociative excitation and dissociative ionization. The dissociative excitation channels are divided into contributions from principal quantum numbers 1–4. For dissociative ionization, the fully differential cross section is calculated using a formally exact expression. These results are compared with approximate expressions. The Born-Oppenheimer expression for the dissociative ionization amplitude is shown to be deficient near onset. A Born-Oppenheimer approximation to the final state is shown to give accurate results for the sharing of kinetic energy between the electronic and the internuclear degrees of freedom—the doubly differential cross section. To accurately calculate the triply differential cross section, including the angular behavior, it is shown that nonadiabatic wave functions for both initial and final states are required at low electron energies.

I. INTRODUCTION

The H_2^+ cation is the smallest molecule, and one that is relevant in contexts ranging from interstellar chemistry [1,2] to fusion reactors and, as such, is well studied in the literature. It provides the one-electron archetype for fundamental processes, such as dissociative recombination [2]. Due to its size, it is tractable to include nonadiabatic effects in calculating its dynamics [3,4]. Such studies provide insight into how coupled electronic and nuclear dynamics may be manipulated by laser light, and in recent years, the interest in strong field and ultrafast physics has led to many experimental and numerical studies on this topic, including accurate descriptions of charge localization [5,6], various processes in strong fields [7–11], and others [12,13]. Benchmark calculations of bound-state rovibronic energies have been given in Refs. [14–19].

The fundamental one-photon processes in H_2^+ may be called excitation, dissociative excitation, and dissociative ionization. The first, excitation to bound vibrational states of excited Born-Oppenheimer electronic states, occurs with vanishing probability from the ground rovibrational state. Dissociative excitation or photodissociation has been studied experimentally [20–23] and theoretically [23–26]. Dissociative ionization has received prior interest by theoreticians over the decades [27–31] and, recently, through the topic [32] of differential cross sections and interference effects [33–37].

Given the degree to which it is studied, it is surprising that no *ab initio* calculation of its one-photon Fermi's golden rule breakup cross section that treats the nuclear and electronic degrees of freedom on the same footing has been published. The process represents one of the three fundamental Coulomb breakup problems, the others including double ionization of helium, a complete calculation of which was reported in 2005 [38]. Here, such calculations are presented.

II. HAMILTONIAN AND BASIS

The calculations employ an implementation [39–42] of the full nonadiabatic Hamiltonian in prolate spheroidal coordinates [4,42]. The nuclear basis set is identical to that used in Ref. [42], but the expressions for the matrix elements have been improved. The basis functions are localized piecewise polynomials defined on a product grid in the prolate spheroidal coordinates with some matrix elements evaluated within the discrete variable representation approximation [43–46]. For odd-$\mathcal{M}$ values, the basis functions include (unitless) factors of $\rho = \sqrt{(\xi^2 - 1)(1 - \eta^2)}$ to enforce square-root boundary conditions.

The exact nonrelativistic Hamiltonian may be written [47]

$$\hat{H} = -\frac{1}{2\mu_e R^2}\nabla^2 + \frac{1}{R} - \frac{1}{r_A} - \frac{1}{r_B} + \frac{1}{\mu_R}$$
$$\times \left[\hat{T}_R + \frac{J(J+1) - 2J_z^2 + \hat{J}^+\hat{l}^- + \hat{J}^-\hat{l}^+ + \hat{l}^2}{2R^2} \right],$$
$$\mu_e = \frac{2 \times 1836.152\,701}{2 \times 1836.152\,701 + 1}, \quad \mu_R = \frac{1}{2}1836.152\,701, \quad (1)$$

with the interparticle distances R, r_A, and r_B, with ∇^2 the Laplacian in the electronic coordinates, and J_z the projection of angular momentum (total J, and electronic l; the projection of nuclear angular momentum is zero) upon the bond axis, conjugate to the third Euler angle γ. Except for ∇^2, operators are denoted with hats, and scalars have no hats in this equation. For $R^{5/2}$ times the wave function, the nuclear kinetic energy may be written

$$\hat{T}_R = -\frac{1}{2}\frac{\partial^2}{\partial R^2} + \left(\frac{1}{R}\frac{\partial}{\partial R} - \frac{1}{2R^2} \right)\left(\hat{Y} + \frac{3}{2} \right)$$
$$- \frac{1}{2R^2}\left(\hat{Y} + \frac{3}{2} \right)^2, \quad (2)$$

in which expression,

$$\hat{Y} = \frac{1}{\xi^2 - \eta^2}\left(\xi(\xi^2 - 1)\frac{\partial}{\partial \xi} + \eta(1 - \eta^2)\frac{\partial}{\partial \eta} \right). \quad (3)$$

It may be shown that

$$(\xi^2 - \eta^2)[(\hat{Y} + 3/2)(\hat{Y} + 3/2) + l^2]$$
$$= \frac{9}{4}(\xi^2 - \eta^2) + \frac{\partial}{\partial \xi}(\xi^4 - \xi^2)\frac{\partial}{\partial \xi} + \frac{\partial}{\partial \eta}(\eta^2 - \eta^4)\frac{\partial}{\partial \eta}$$
$$+ J_z^2(\xi^2 - \eta^2)\left(1 + \frac{(\xi\eta + \alpha)^2}{(\xi^2 - 1)(1 - \eta^2)}\right), \qquad (4)$$

in which the second derivatives $\frac{\partial^2}{\partial\xi\partial\eta}$ cancel each other and more trivially that

$$(\xi^2 - \eta^2)\left(\hat{Y} + \frac{3}{2}\right) = \left[\xi(\xi^2 - 1)\frac{\partial}{\partial\xi} - \frac{1}{2} + \frac{3\xi^2}{2}\right]$$
$$- \left[\eta(\eta^2 - 1)\frac{\partial}{\partial\eta} - \frac{1}{2} + \frac{3\eta^2}{2}\right]. \qquad (5)$$

The raising and lowering operators are

$$l^{\pm} = \pm e^{\pm i\phi}\frac{\rho}{\xi^2 - \eta^2}\left(\eta\frac{\partial}{\partial\xi} - \xi\frac{\partial}{\partial\eta}\right) + i\frac{\xi\eta}{\rho}\frac{\partial}{\partial\phi}. \qquad (6)$$

As mentioned above, the primitive basis functions are defined with factors of $\rho = \sqrt{(\xi^2 - 1)(1 - \eta^2)}$ for odd $\mathcal{M}$. The matrix elements of the raising and lowering operators for a bra-ket with the ket having even quantum number $\mathcal{M}$, therefore, involve integrals of the following operator with respect to the polynomial basis functions:

$$\rho(\xi^2 - \eta^2)l^{\pm} = \pm\left((1 - \eta^2)\eta\left[(\xi^2 - 1)\frac{\partial}{\partial\xi} + \xi\right]\right.$$
$$\left. -(\xi^2 - 1)\xi\left[(\eta^2 - 1)\frac{\partial}{\partial\eta} + \eta\right]\right)$$
$$- (\mathcal{M} \pm 1)\xi\eta. \qquad (7)$$

The matrix elements involving an odd-$\mathcal{M}$ ket are, in turn, expressed in terms of matrix elements of the operator,

$$(\xi^2 - \eta^2)l^{\pm}\rho = \pm(\cdots) - \mathcal{M}\xi\eta. \qquad (8)$$

The matrix elements of the individual terms in Eq. (4), which are Hermitian, of the operator in Eqs. (5) and (8) that occurs both in η and in ξ, which is anti-Hermitian, and of the anti-Hermitian $(\frac{1}{R}\frac{\partial}{\partial R} - \frac{1}{2R^2})$ operator are integrated exactly by quadrature. As in Refs. [39,42], only one-dimensional integrals are involved, and therefore the matrix representations of these operators are quite sparse.

The basis set employs exterior complex scaling [48–54] of the electronic and nuclear coordinates in order to enforce outgoing wave boundary conditions exactly. The coordinates of electrons and nuclei are rotated into the complex coordinate plane in the asymptotic region, which results in an anti-Hermitian component of the Hamiltonian that only absorbs outgoing flux. Bound states are not absorbed, and despite the fact that Rydberg states penetrate into the complex scaled region, their analytic continuations are accurately represented, obeying an orthogonality relationship, having unperturbed real eigenvalues, etc.

III. TOTAL CROSS SECTIONS

The absorption cross section is calculated [54–56] by solving the linear equation,

$$\psi^{sc}(\omega) = \hat{G}^+(E_0 + \omega)\mu\psi_0, \qquad (9)$$

in which E_0 is the energy of the initial ground rovibronic eigenstate ψ_0, ω is the photon energy, μ is the dipole operator, and $\hat{G}^+(E_0 + \omega)$ is the outgoing wave Green's function as represented by exterior complex scaling.

Examples of the calculated time-independent half-scattering wave functions ψ^{sc} are shown in Fig. 1. The wave functions are evaluated parallel or perpendicular to the bond axis for the corresponding laser polarizations, i.e., at the point $\eta = \pm 1$ or 0, correspondingly. At the energies studied, the behavior in η is mostly uninteresting, being mostly p-wave outgoing flux for dissociative ionization, for instance.

To extract the cross sections from the ψ^{sc}, the method of Ref. [57] as adapted to exterior complex scaling in Ref. [42] is applied. As the outgoing wave at a given photon energy is directly calculated via Eq. (9), no Fourier transform is needed. The total breakup cross section is obtained in the length gauge and for polarization parallel to the bond axis via

$$\sigma(\omega) = \frac{8}{3}\pi\alpha\omega\hbar\langle\psi^{sc}(\omega)|a(\hat{H})|\psi^{sc}(\omega)\rangle, \qquad (10)$$

with α the fine structure constant. In this expression, $a(\hat{H}) \equiv \frac{1}{2}(\hat{H} - \hat{H}^{\dagger})$ is the anti-Hermitian part of the Hamiltonian, the Hermitian part being $h(\hat{H}) \equiv \frac{1}{2}(\hat{H} + \hat{H}^{\dagger})$. This is an isotropic cross section, so there is the factor of $\frac{1}{3}$. For perpendicular polarization, there is a factor of $\frac{2}{3}$, and so the corresponding coefficient in Eq. (10) is $\frac{16}{3}$.

To distinguish dissociative excitation from dissociative ionization, the anti-Hermitian part of the Hamiltonian is divided into the part that absorbs flux for large bond lengths R and that which does so for large values of the prolate spheroidal coordinate ξ. With the identity

$$\frac{1}{r_A} + \frac{1}{r_B} = \frac{4\xi}{R(\xi^2 - \eta^2)}, \qquad (11)$$

and the shorthand

$$B = -\frac{1}{2\mu_e}\nabla^2 + \frac{1}{2\mu_R}\left[\left(Y + \frac{3}{2}\right)^2 + \hat{l}^2\right],$$
$$V = -\frac{4\xi}{\xi^2 - \eta^2}, \quad D = \frac{1}{\mu_R}\left(\frac{1}{R}\frac{\partial}{\partial R} - \frac{1}{2R^2}\right), \qquad (12)$$
$$T = -\frac{1}{2}\frac{\partial^2}{\partial R^2} + \frac{1}{R} + \frac{J^2 - 2J_z}{2R^2}, \quad Y = \left(\hat{Y} + \frac{3}{2}\right),$$

the full Hamiltonian may be abbreviated

$$H = \frac{1}{R^2}B + T + \frac{1}{R}V + DY, \qquad (13)$$

and the anti-Hermitian part of the Hamiltonian divided

$$a(H) = H_{\text{anti}}^e + H_{\text{anti}}^R, \qquad (14)$$
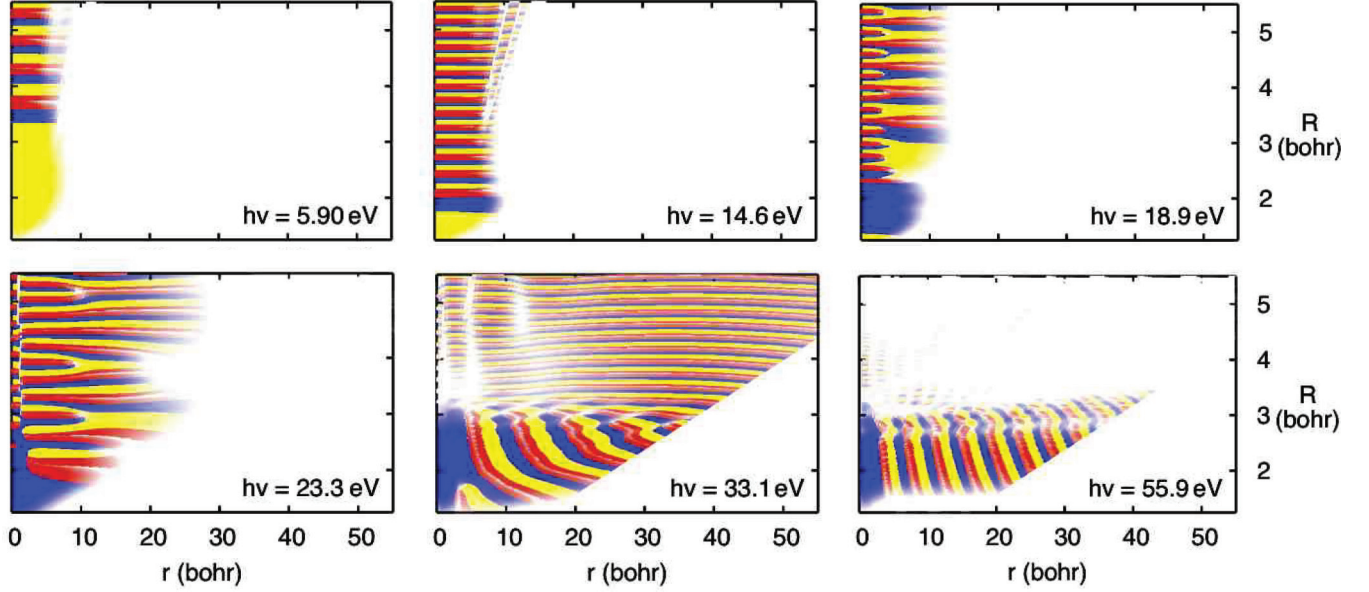
FIG. 1. (Color online) Outgoing waves $\psi^{sc}(\omega)$ for $h\nu = 5.9$, 14.6, 18.95, 23.3, 33.1, and 56.0 eV, evaluated at $\eta = 1$, i.e., along the bond axis. The behavior of the wave function is trivial in the η coordinate. The modulus is plotted on a logarithmic scale, and the color denotes the phase with the dark-medium-light (blue-red-yellow) colors having time derivatives light-dark-medium (yellow-blue-red). The coordinates are real valued within the plots.

such that

$$H_{\text{anti}}^e = h\left(\frac{1}{R^2}\right)a(B) + h\left(\frac{1}{R}\right)a(V) + a(D)h(Y),$$

$$H_{\text{anti}}^R = a\left(\frac{1}{R^2}\right)h(B) + a(T) + a\left(\frac{1}{R}\right)h(V) + h(D)a(Y). \tag{15}$$

The cross sections for dissociative ionization $\sigma^{DI}(E)$ and dissociative excitation $\sigma^{DE}(E)$ are calculated as

$$\sigma^{DI}(\omega) = \tfrac{8}{3}\pi\alpha\omega\hbar\langle\psi^{sc}(\omega)|H_{\text{anti}}^e|\psi^{sc}(\omega)\rangle,$$

$$\sigma^{DE}(\omega) = \tfrac{8}{3}\pi\alpha\omega\hbar\langle\psi^{sc}(\omega)|H_{\text{anti}}^R|\psi^{sc}(\omega)\rangle, \tag{16}$$

with $\sigma(\omega) = \sigma^{DI}(\omega) + \sigma^{DE}(\omega)$.

In Fig. 2, the cross sections $\sigma(E)$, $\sigma^{DI}(E)$, and $\sigma^{DE}(E)$ are plotted. The total cross section is also calculated via the optical theorem, i.e.,

$$\sigma(\omega) = -\tfrac{4}{3}\pi\alpha\omega\hbar\,\text{Im}(\langle\mu\psi_0|\hat{G}^+(E_0 + \omega)|\mu\psi_0\rangle). \tag{17}$$

The agreement between the two formally equivalent results is essentially exact (to approximately five to eight significant figures, in general), although they are calculated quite differently.

It is true that there may be outgoing flux that is absorbed in the region in which both H_{anti}^R and H_{anti}^e are nonzero, calling into question the separation described above. However, the results for σ^{DI} and σ^{DE} presented here are converged with respect to the complex scaling radii in both the electronic and nuclear coordinates.

IV. DISSOCIATIVE EXCITATION

The dissociative excitation cross section σ^{DE} is divided into contributions of the final electronic states of the hydrogen atom. The wave function is projected upon the fixed-nuclei electronic eigenfunctions ϕ_i,

$$\psi_i^{sc}(\xi,\eta,R;\omega) = \phi_i(\xi,\eta;R)\int(\xi'^2 - \eta'^2)d\xi'd\eta'$$

$$\times\phi_i(\xi',\eta';R)\psi^{sc}(\xi',\eta',R;\omega). \tag{18}$$

The division of the cross section proceeds via

$$\sigma_{ij}^{DE}(\omega) = \tfrac{8}{3}\pi\alpha\omega\hbar\langle\psi_i^{sc}(\omega)|H_{\text{anti}}^R|\psi_j^{sc}(\omega)\rangle, \tag{19}$$

such that $\sum_{ij}\sigma_{ij}^{DE}(\omega) = \sigma^{DE}(\omega)$.

If the final states ϕ_j were exact representations of the asymptotic states and in the limit of large projection radius, σ_{ii}^{DE} of Eq. (19) would be the formally exact cross section for Rydberg state i; the off-diagonal results σ_{ij}, $i \neq j$, would go to zero.

A. Formal and numerical considerations

However, because the prolate spheroidal coordinate R is not exactly the same as the dissociative coordinate, due to the mass of the electron, states $\phi_i(R)$ that are used for the projection are not exactly the asymptotic states; the asymptotic states are delocalized in R. Due to the resulting nonadiabatic coupling between the approximate states $\phi_i(R)$, nonzero off-diagonal results σ_{ij}, $i \neq j$, are expected.

Nonzero off-diagonal contributions are also expected if the projection is not performed at a sufficiently large bond radius R such that the different principal quantum number manifolds are still significantly mixed by the interaction with the bare proton. In any case, the off-diagonal cross sections σ_{ij}, $i \neq j$, are
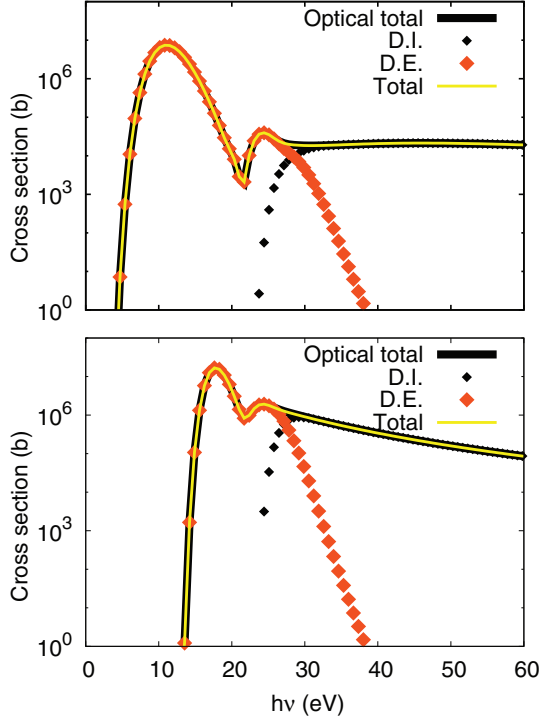
FIG. 2. (Color online) Cross sections calculated for total breakup $\sigma(\omega)$, light colored lines, dissociative ionization $\sigma^{DI}(\omega)$, black small diamonds, and dissociative excitation $\sigma^{DE}(\omega)$, large orange (pale) diamonds, as calculated via Eqs. (10) and (16), and total absorption via the optical theorem, Eq. (17), thick black lines, for parallel (top) and perpendicular (bottom) polarization.

spurious and should be significantly smaller than the physical cross sections σ_{ii} for the latter to be regarded as reliable.

The projection onto final Rydberg states must be performed at a bond length large enough such that there are no significant nonadiabatic couplings from that bond length outward. The last avoided crossing involving a Σ_u $n = 3$ electronic state occurs at approximately $16.5a_0$, and that involving a Π_u $n = 4$ state occurs at approximately $15a_0$. The calculations are observed to be well converged with an exterior complex scaling bond length slightly larger than these values. The last avoided crossing involving the $n = 4$ Σ_u states occurs at approximately $40a_0$, and projection upon these states was not attempted.

B. Results

Results are shown in Fig. 3. This figure shows the dissociative excitation cross section binned by the principal quantum number of the final Rydberg state. The electronic orbital angular momentum of the final Rydberg state is not resolved. The total cross section into the principal quantum number n, σ_n^{DE} with one subscript, is defined as

$$\sigma_n^{DE} = \sum_{i \in n} \sum_{j \in n} \sigma_{ij}^{DE}, \qquad (20)$$

with the sums of spurious cross sections off-diagonal in the principal quantum number denoted

$$\tilde{\sigma}_n^{DE} = \sum_{i \in n} \sum_{j \notin n} \sigma_{ij}^{DE}, \qquad (21)$$
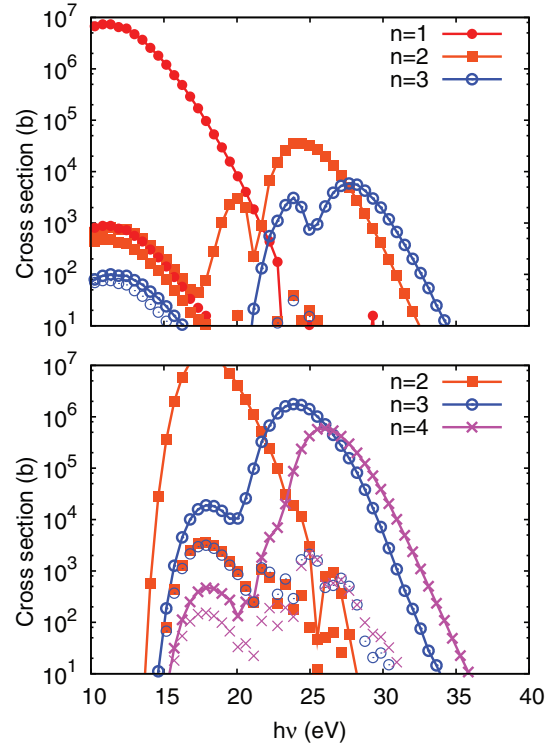
FIG. 3. (Color online) Cross sections σ_n [Eq. (20), connected dots] for dissociative excitation into the manifold of Rydberg states with principal quantum number n and sums of unphysical erroneous of-diagonal cross sections $\tilde{\sigma}_n$ [Eq. (21), dots] as described in the text. Top, parallel polarization; bottom, perpendicular.

in which the notation $\sum_{i \in n}$ means sum over fixed-nuclei states i that correlate with a given principal quantum number n. As discussed, the off-diagonal sum $\tilde{\sigma}_n^{DE}$ should be regarded as a minimum error bound to the calculated physical cross section σ_n^{DE}.

As can be seen in Fig. 3, the largest part of the dissociative excitation cross section is the low-energy part due to absorption into the lowest $1\,\Sigma_u$ and $1\,\Pi_u$ states. About 4 orders of magnitude below the peak cross sections, at about 10 and 18 eV, respectively, one may see that there are nonzero cross sections, both diagonal and off-diagonal, calculated for the higher electronic states. These are nonzero below their thresholds and are congruent to the dominant $1\,\Sigma_u$ or $1\,\Pi_u$ peak. These facts suggest that these calculated features are spurious and probably come from contamination of the higher states' results from the outgoing flux in the lowest electronic state channel. As explained above, the electronic states used for the final-state projection in dissociative excitation are not precisely the long-range states, and therefore, this behavior is not surprising.

At higher energies, the calculated physical cross sections σ_n^{DE} in Fig. 3 are several orders of magnitude above any unphysical off-diagonal results and, therefore, should be regarded as reliable. Nonadiabatic coupling leads to double peaks, which are especially prominent in parallel polarization; the main peak for each final principal quantum number has a small side peak at lower energies due to coupling from the
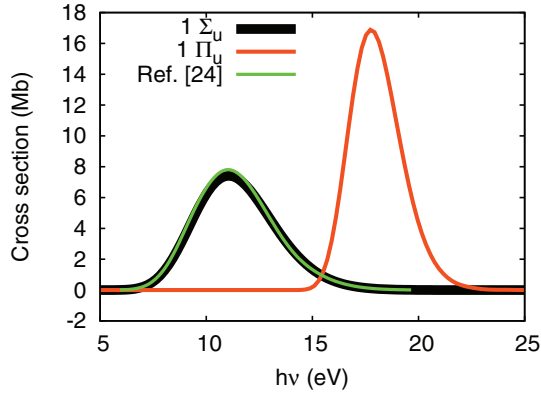
FIG. 4. (Color online) Photodissociation cross sections for dissociative excitation into the $1s\ \Sigma_u$ and $2p\ \Pi_u$ electronic states as calculated presently and as calculated for $1s\ \Sigma_u$ in Ref. [24].

high-energy side of the peak of the prior principal quantum number.

The prior experimental results [20–23] on the photodissociation of H$_2^+$ do not permit a comparison with the present calculation. Calculated cross sections for the lowest $1s\ \Sigma_u$ photodissociation [24–26] and that of the $2p\ \Pi_u$ [26] have been reported. In Fig. 4, the cross sections calculated for these final states are shown and that of the Σ_u is shown to compare well with the result of Dunn calculated near the peak of the cross section within the Born-Oppenheimer approximation [24]. On this linear scale, the nonadiabatic contributions are not visible.

V. DISSOCIATIVE IONIZATION

The dissociative ionization flux at a given photon energy may be differentiated with respect to the energy sharing between the electronic and nuclear degrees of freedom and with respect to the angular behavior. The dissociative ionization cross section is obtained by calculating the amplitudes $A_l(k,\kappa)$ for breakup as a function of kinetic-energy sharing and electronic angular momentum quantum number,

$$A_l(k,\kappa) = \langle \Psi_l^-(k,\kappa)|\mu|\Psi^0\rangle. \tag{22}$$

Presently amplitudes $A_l(k,\kappa)$ are calculated exactly and by using two degrees of approximation as described below.

A. Exact and approximate amplitude expressions

For the fixed-nuclei problem, exact final states were calculated in Ref. [39] by solving the equation

$$\Psi_l^-(E) = \phi_0 + G^+(E)(H-E)\phi_0, \tag{23}$$

with the zeroth-order wave function a Coulomb wave $\phi_0 = f_l(kr)P_{lm}(\cos\theta)$, $E = \frac{k^2}{2}$, and the interaction term is

$$(H-E)\phi_0 = \left(\frac{1}{r} - \frac{1}{r_A} - \frac{1}{r_B}\right)\phi_0. \tag{24}$$

In contrast, for three-body scattering with pairwise interactions Eq. (23) is not valid. As an alternative to employing an explicit representation of $\Psi^-(E)$, stationary phase expressions [58,59] that can be implemented in a numerically robust way
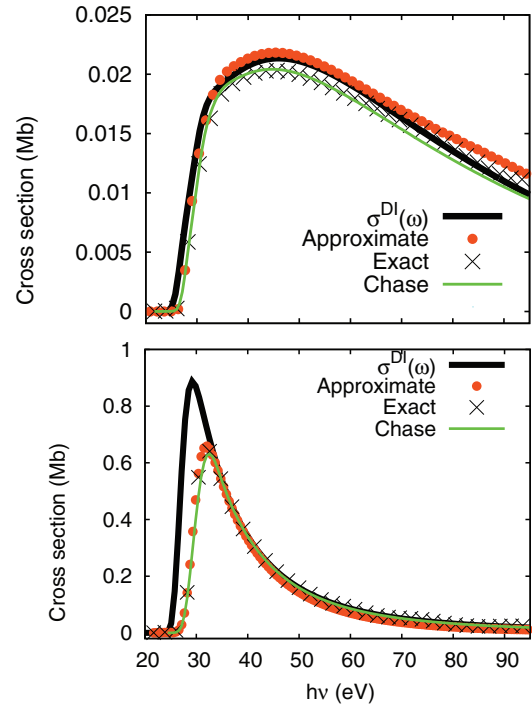
FIG. 5. (Color online) Total cross sections for dissociative ionization calculated in different ways: using the flux expression Eq. (16); using Eq. (22) and integrating Eq. (26) with respect to energy sharing; using the exact states of Eq. (25), the approximate final states of Eq. (27), or the Chase approximation with Born-Oppenheimer amplitudes Eq. (28). Top: parallel polarization; bottom: perpendicular.

[54–56] have been applied to three-body Coulomb breakup problems with two electrons.

However, the prolate spheroidal coordinate system, along with the unequal masses between the electronic and nuclear degrees of freedom, in general appears to allow Eq. (23) to be implemented such that it yields an accurate final state. At the end of the electronic grid in prolate spheroidal coordinates, the electron is always at a greater radius than the nuclei. Thus, we should not expect to be able to construct final states for which $\mu_R k < \mu_e \kappa$ for which the protons recoil faster than the electrons and are thereby shielded from one another by the electron. Given a maximum of approximately 13.6-eV nuclear
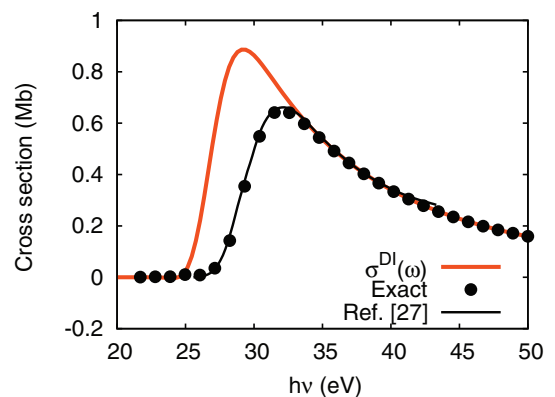
FIG. 6. (Color online) Dissociative ionization cross section calculated exactly using Eq. (16) and as in Ref. [27].

kinetic-energy release, this would indicate that our results are certainly good above 7.5-meV electron energy, a quantity that is not visible in any of the figures.

The final-state wave function is thereby calculated as

$$\Psi_l^-(k,\kappa) = f_l(kr)f_1(\kappa R) + G^+(E)(H - E)f_l(kr)f_1(\kappa R),$$

$$(25)$$

wherein $f_l(kr)$ and $f_1(\kappa R)$ are attractive ($Z = 2$) and repulsive ($Z = 1$) Coulomb functions in the electronic and nuclear degrees of freedom, energy normalized. This is performed in the same manner as in Ref. [39]. The final-state wave functions so constructed are orthogonal to the bound rovibronic states for $\mathcal{M} = 0$ and 1 to within no more than one part in 10^3, in general.

With the amplitudes defined as per Eq. (22), cross sections differential in the kinetic-energy sharing between the electron $\frac{k^2}{2} = \epsilon$ and that of the nuclei $\frac{\kappa^2}{2} = E$ at constant total energy $E + \epsilon$ are

$$\left.\frac{\partial}{\partial E}\sigma(E,\epsilon)\right|_{E+e} = \frac{4}{3}\pi^2\alpha\omega m\sum_l |A_l(k,\kappa)|^2, \quad (26)$$

wherein $\Psi^-(k,\kappa)$ is energy normalized.

Approximate final states are often employed in calculations in the literature, and in some contexts, simple unperturbed product wave functions ϕ_0 are surprisingly accurate. For instance, in time-dependent calculations on small atoms and diatomics, cross sections may be calculated [60–63] by projecting a propagated wave packet onto unperturbed Coulomb wave functions as long as enough time has elapsed such that the ionized electrons have escaped beyond the molecule. In systems containing resonances, this method becomes less tractable the longer lived the resonances. A comparison of different amplitude expressions for single and double ionization of two-electron systems, similar to that
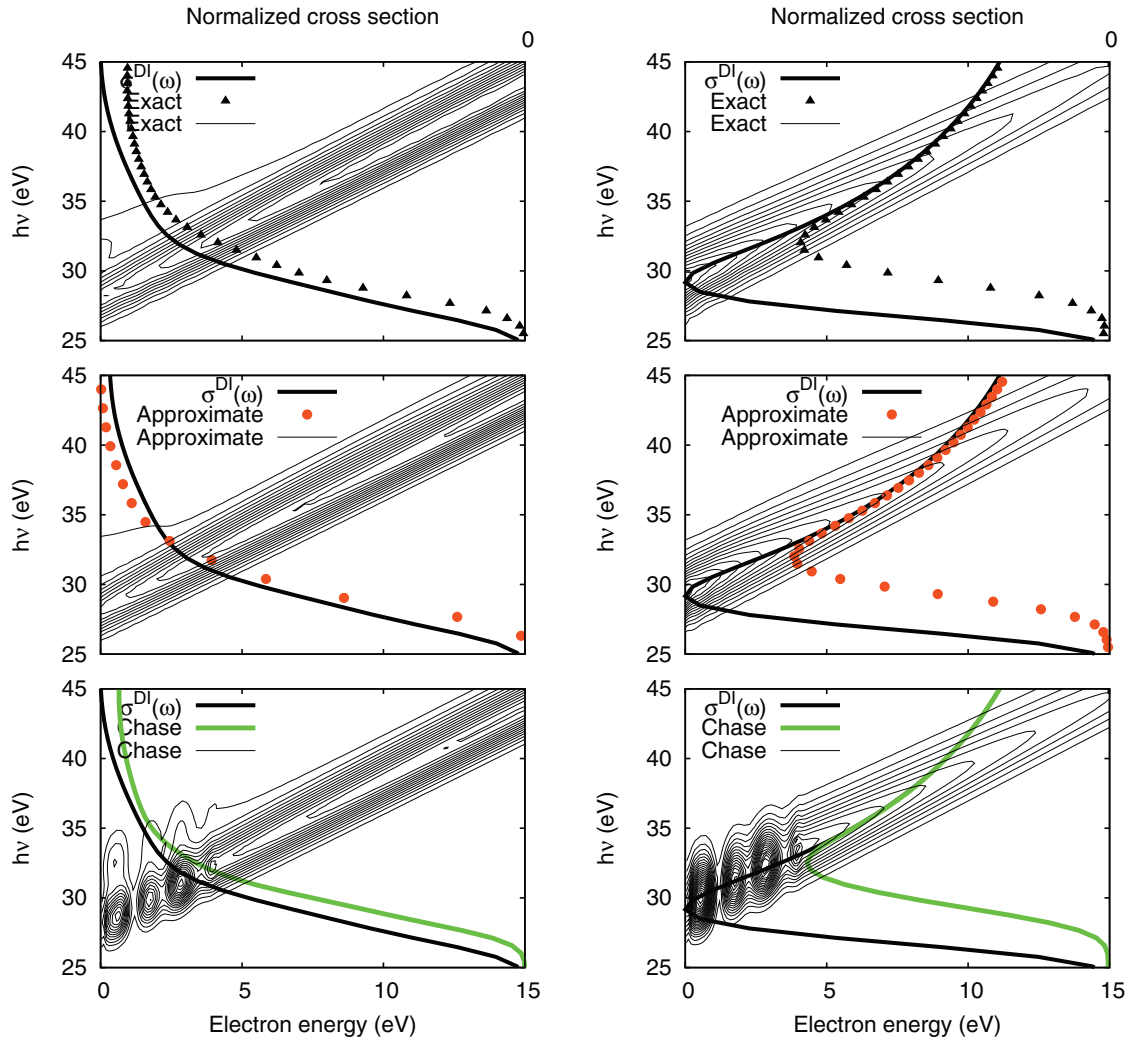
FIG. 7. (Color online) Distributions of kinetic energy between the electron and the nuclei calculated exactly (top) using Born-Oppenheimer final states (middle) and using Born-Oppenheimer initial and final states (bottom, Chase approximation). The cross-section differential in energy sharing, Eq. (26), is plotted with contours as a function of electron energy and photon energy. The total cross section, without regard to energy sharing, is plotted vertically as a function of photon energy. The result of integrating the differential cross section is plotted with different styles as in Fig. 5, and the dissociative ionization cross section as calculated via Eq. (16) is plotted in bold black.
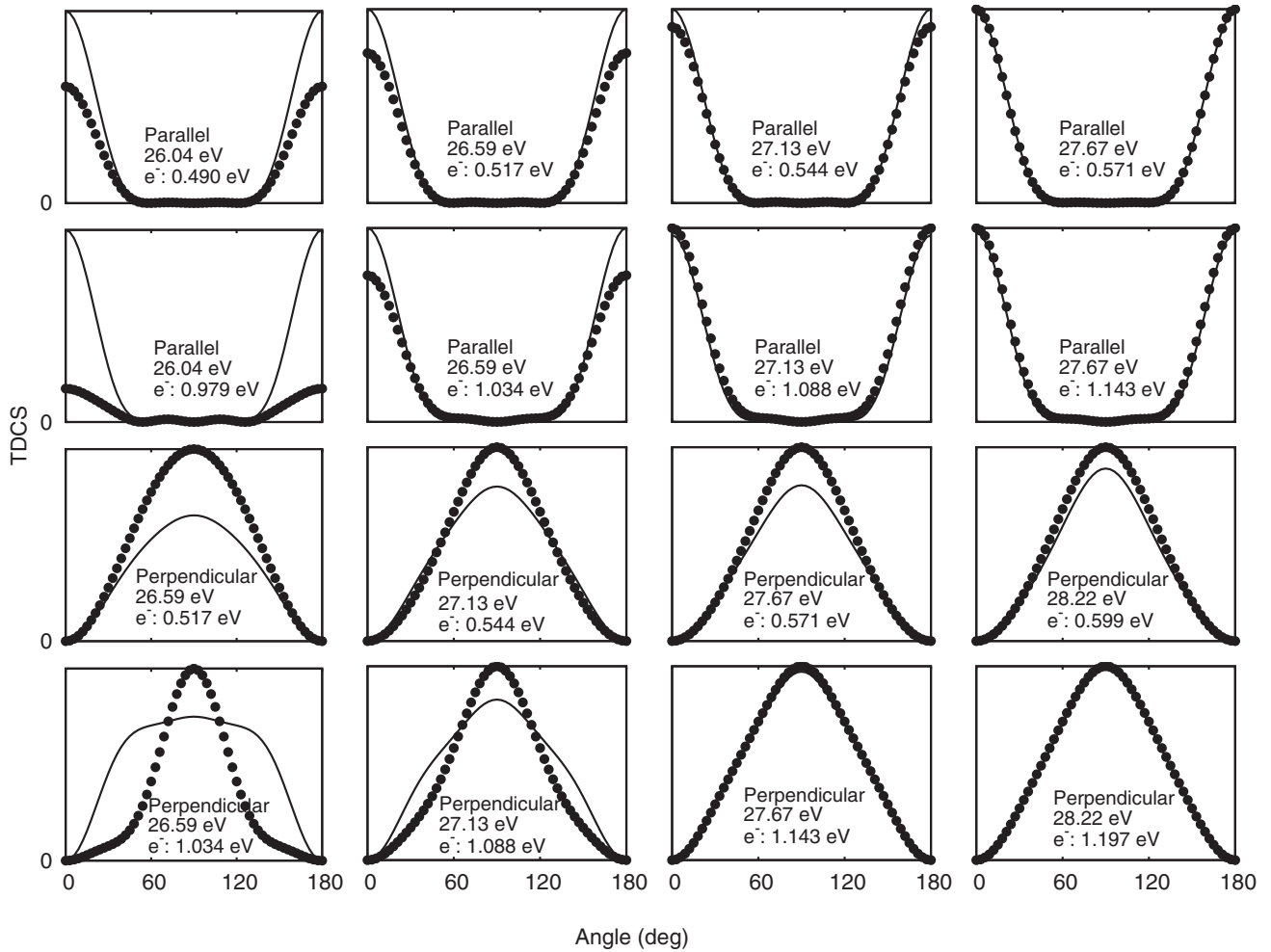
FIG. 8. Triply differential cross sections for dissociative photoionization calculated exactly (dots) and with approximate final states (lines) with each panel plotted on an arbitrary scale, the two results in each panel internormalized. In each panel, the photon energy and the outgoing electron energy are indicated.

presented here for dissociative ionization of H$_2^+$, can be found in Ref. [64].

Approximate final states $\Psi_l^-(k,\kappa)$ are constructed as products

$$\Psi_l^-(k,\kappa) \approx f_1(\kappa R)\psi_l^-(k^2/2; R) \qquad (27)$$

of Coulomb waves in the bond distance and the exact fixed-nuclei scattering state ψ^-. This is, therefore, a Born-Oppenheimer representation of the final state. Finally, the initial state is replaced with its Born-Oppenheimer approximation as well such that the amplitudes are the matrix elements of the Born-Oppenheimer amplitudes with respect to the initial and final vibrational states, which expression is called the Chase approximation [65],

$$A_l(k,\kappa) \approx \int dR\, f_1(\kappa R)\chi_0(R)A_l(k; R), \qquad (28)$$

in which χ_0 is the ground vibrational Born-Oppenheimer state.

B. Results

Cross sections for dissociative ionization are shown in Fig. 5. For these total cross sections, there is very little

difference among the various results calculated using the different amplitude expressions, exact and approximate. However, in perpendicular polarization, there is a large discrepancy between these results and $\sigma^{DI}(\omega)$ as defined by Eq. (16). The origin of this discrepancy is unclear, but it calls into question the division of the cross section as defined by that equation. Further study of this discrepancy is, therefore, indicated. The results calculated via the amplitude expressions should be regarded as reliable due to the fact that one of them has been calculated in a formally exact manner.

The dissociative ionization cross section is compared to the calculation of Ref. [27], the exact analytic fixed-nuclei result convolved over the initial vibrational wave function in Fig. 6. This and the present calculation are also in agreement with the prior Born-Oppenheimer results [28–31]. The cross section is overwhelmingly dominated by the perpendicular component, and the perpendicular component of the total dissociative ionization cross section is affected little by inclusion of the internuclear coordinate.

The distributions of kinetic energy between the electrons and the nuclei are shown in Fig. 7. In these figures the exact, approximate, and Born-Oppenheimer (Chase approximation)

results are compared. One can see that for electron energies above 5 eV, the three results are substantially in agreement. Below 5 eV, however, the Chase approximation yields qualitatively incorrect behavior, yielding strong minima in the cross section as a function of energy sharing, whereas in the exact result, there are none. In terms of the distribution of kinetic energy between the electron and the nuclei, the results for approximate Born-Oppenheimer final states do not significantly differ from the exact ones.

However, when the full triply differential cross section (TDCS) is calculated, there are clear differences, indicating that an exact nonadiabatic treatment is indeed necessary to fully describe the breakup of H_2^+. In Fig. 8, the triply differential cross section, differential with respect to energy, energy sharing, and the relative angle of ionization and dissociation, is plotted near onset and for low electron energies. In general, in parallel polarization, these figures show that the approximate treatment with Born-Oppenheimer final states somewhat overestimates these low electron kinetic-energy cross sections. However, the shape of the TDCS for parallel polarization—that is to say, the relative magnitude and phases of the partial waves contributing to it—is in agreement and is nearly constant over all energies for both treatments. In contrast, for perpendicular polarization there are substantial differences in the shape of the TDCS obtained via the exact and approximate final-state treatments. This indicates that nonadiabatic effects

are important for a completely accurate description of the dynamics.

VI. CONCLUSION

Full nonadiabatic calculations of the cross sections for the breakup of the H_2^+ cation by photon impact have been presented. In the case of dissociative ionization, the exact result has been critically compared to approximate ones, and it was shown that the Born-Oppenheimer approximation gives cross-sections differential in energy sharing that are very close to the exact result. However, an accurate calculation of the fully differential cross section requires the full nonadiabatic treatment. The use of the described flux formalism to calculate the dissociative ionization of the cross section, Eq. (16), is called into question due to its disagreement with the formally exact result in perpendicular polarization. In the case of dissociative excitation, the cross sections have been calculated over six orders of magnitude, revealing the influence of nonadiabatic coupling.

[1] A. Dalgarno, E. Herbst, S. Novick, and W. Klemperer, Astrophys. J. **183**, L131 (1973).

[2] T. Takagi, Phys. Scr. **T96**, 52 (2002).

[3] I. Kawata, H. Kono, and Y. Fujimura, J. Chem. Phys. **110**, 11152 (1999).

[4] B. D. Esry and H. R. Sadeghpour, Phys. Rev. A **60**, 3604 (1999).

[5] K. Liu, W. Hong, Q. Zhang, and P. Lu, Opt. Express **19**, 26359 (2011).

[6] K. Liu, Q. Zhang, and P. Lu, Phys. Rev. A **86**, 033410 (2012).

[7] T. K. Kjeldsen, L. B. Madsen, and J. P. Hansen, Phys. Rev. A **74**, 035402 (2006).

[8] A. K. Paul, S. Adhikari, D. Mukhopadhyay, G. J. Halasz, A. Vibok, R. Baer, and M. Baer, J. Phys. Chem. A **113**, 7331 (2009).

[9] V. S. Prabhudesai, U. Lev, A. Natan, B. D. Bruner, A. Diner, O. Heber, D. Strasser, D. Schwalm, I. Ben-Itzhak, J. J. Hua *et al.*, Phys. Rev. A **81**, 023401 (2010).

[10] X. Guan, E. B. Secor, K. Bartschat, and B. I. Schneider, Phys. Rev. A **84**, 033420 (2011).

[11] V. Roudnev and B. D. Esry, Phys. Rev. A **71**, 013411 (2005).

[12] J. Zhao and Z. Zhao, Phys. Rev. A **78**, 053414 (2008).

[13] B. Moser and G. N. Gibson, Phys. Rev. A **80**, 041402 (2009).

[14] C. L. Beckel, B. D. Hansen III, and J. M. Peek, J. Chem. Phys. **53**, 3681 (1970).

[15] C. L. Beckel, M. Shafi, and J. M. Peek, J. Chem. Phys. **59**, 5288 (1973).

[16] A. S. Kiametis, F. M. Vieira, A. L. A. Fonseca, G. M. e Silva, and R. Gargano, Int. J. Quantum Chem. **108**, 2398 (2008).

[17] A. S. Kiametis, T. A. M. Matheus, A. L. A. Fonseca, G. M. e Silva, and R. Gargano, Int. J. Quantum Chem. **111**, 1316 (2011).

[18] H. V. R. Vila, L. A. Leal, A. L. A. Fonseca, and R. Gargano, Int. J. Quantum Chem. **112**, 829 (2012).

[19] J. M. Taylor, Z.-C. Yan, A. Dalgarno, and J. F. Babb, Mol. Phys. **97**, 25 (1999).

[20] F. von Busch and G. H. Dunn, Phys. Rev. A **5**, 1726 (1972).

[21] J.-B. Ozenne, D. Pham, and J. Durup, Chem. Phys. Lett. **17**, 422 (1972).

[22] N. P. F. B. van Asselt, J. G. Maas, and J. Los, Chem. Phys. **5**, 429 (1974).

[23] J.-B. Ozenne, J. Durup, R. W. Odom, C. Pernot, A. Tabche-Fouhaille, and M. Tadjeddine, Chem. Phys. **16**, 75 (1976).

[24] G. H. Dunn, Phys. Rev. **172**, 1 (1968).

[25] J. D. Argyros, J. Phys. B **7**, 2025 (1974).

[26] S. Saha, K. K. Datta, D. Basu, and A. K. Barau, J. Phys. B **13**, 3755 (1980).

[27] D. R. Bates, U. Opik, and G. Poots, Proc. Phys. Soc., London Sect. A **66**, 1113 (1953).

[28] D. R. Bates and U. Opik, J. Phys. B **1**, 543 (1968).

[29] T. N. Rescigno and C. W. McCurdy, Phys. Rev. A **31**, 624 (1985).

[30] J. A. Richards and F. P. Larkins, J. Phys. B **19**, 1945 (1986).

[31] M. Morita and S. Yabushita, J. Comput. Chem. **29**, 2471 (2008).

[32] H. D. Cohen and U. Fano, Phys. Rev. **150**, 30 (1966).

[33] R. DellaPicca, P. D. Fainstein, M. L. Martiarena, and A. Dubois, Phys. Rev. A **75**, 032710 (2007).

[34] J. Fernandez, O. Fojon, A. Palacios, and F. Martin, Phys. Rev. Lett. **98**, 043005 (2007).

[35] R. DellaPicca, P. D. Fainstein, M. L. Martiarena, and A. Dubois, Phys. Rev. A **77**, 022702 (2008).

[36] J. Colgan, A. Huetz, T. J. Reddish, and M. S. Pindzola, J. Phys. B **41**, 085202 (2008).

[37] X. Guan, E. B. Secor, K. Bartschat, and B. I. Schneider, Phys. Rev. A **85**, 043419 (2012).

[38] T. N. Rescigno, M. Baertschy, W. A. Isaacs, and C. W. McCurdy, Science **286**, 2474 (1999).

[39] L. Tao, C. W. McCurdy, and T. N. Rescigno, Phys. Rev. A **79**, 012719 (2009).

[40] L. Tao, C. W. McCurdy, and T. N. Rescigno, Phys. Rev. A **80**, 013402 (2009).

[41] L. Tao, C. W. McCurdy, and T. N. Rescigno, Phys. Rev. A **82**, 023423 (2010).

[42] D. J. Haxton, K. V. Lawler, and C. W. McCurdy, Phys. Rev. A **83**, 063416 (2011).

[43] A. S. Dickinson and P. R. Certain, J. Chem. Phys. **49**, 4209 (1968).

[44] G. C. Corey and D. Lemoine, J. Chem. Phys. **97**, 4115 (1992).

[45] J. C. Light, I. P. Hamilton, and J. V. Lill, J. Chem. Phys. **82**, 1400 (1985).

[46] T. N. Rescigno and C. W. McCurdy, Phys. Rev. A **62**, 032706 (2000).

[47] J. Z. H. Zhang, *Theory and Application of Quantum Molecular Dynamics* (World Scientific, Hackensack, NJ, 1999).

[48] J. Aguilar and J. M. Combes, Commun. Math. Phys. **22**, 269 (1971).

[49] E. Balslev and J. M. Combes, Commun. Math. Phys. **22**, 280 (1971).

[50] N. Moiseyev, P. R. Certain, and F. Weinhold, Mol. Phys. **36**, 1613 (1978).

[51] N. Moiseyev and J. O. Hirschfelder, J. Chem. Phys. **88**, 1063 (1987).

[52] N. Lipkin, R. Lefebvre, and N. Moiseyev, Phys. Rev. A **45**, 4553 (1992).

[53] N. Moiseyev, Phys. Rep. **302**, 211 (1998).

[54] C. W. McCurdy, M. Baertschy, and T. N. Rescigno, J. Phys. B **37**, R137 (2004).

[55] M. Baertschy, T. N. Rescigno, and C. W. McCurdy, Phys. Rev. A **64**, 022709 (2001).

[56] C. W. McCurdy and T. N. Rescigno, Phys. Rev. A **62**, 032712 (2000).

[57] A. Jäckle and H.-D. Meyer, J. Chem. Phys. **105**, 6778 (1996).

[58] M. R. H. Rudge, Rev. Mod. Phys. **40**, 564 (1968).

[59] M. R. H. Rudge and M. J. Seaton, Proc. R. Soc. A **283**, 262 (1965).

[60] S. X. Hu, J. Colgan, and L. A. Collins, J. Phys. B **38**, L35 (2005).

[61] M. S. Pindzola, S. A. Abdel-Naby, J. Colgan, and A. Dorn, J. Phys. B **45**, 215208 (2012).

[62] X. Ren, T. Pflüger, S. Xu, J. Colgan, M. S. Pindzola, A. Senftleben, J. Ullrich, and A. Dorn, Phys. Rev. Lett. **109**, 123202 (2012).

[63] R. Pazourek, J. Feist, S. Nagele, and J. Burgdörfer, Phys. Rev. Lett. **108**, 163001 (2012).

[64] L. Argenti, R. Pazourek, J. Feist, S. Nagele, M. Liertzer, E. Persson, J. Burgdörfer, and E. Lindroth, Phys. Rev. A **87**, 053405 (2013).

[65] D. M. Chase, Phys. Rev. **104**, 838 (1956).